Int. J. Electrochem. Sci., 13 **(2018)** 9520 – 9530, doi: 10.20964/2018.10.14

International Journal of
ELECTROCHEMICAL
SCIENCE
www.electrochemsci.org

Fabrication of Hollow $MgFe_2O_4$ Microspheres for High Performance Anode of Lithium Ion Battery

Wenhui Liu , Riya Jin, Yunlu Li, yuanyuan Wu, Xiong Cao, Shuangqi Hu *

Environmental and Safety Engineering Institute, North University of China, Taiyuan, Shanxi 030051, People's Republic of China
*E-mail: hsq@nuc.edu.cn

Received: 13 May 2018 / *Accepted:* 14 July 2018 / *Published:* 1 September 2018

In this work, spinel $MgFe_2O_4$ hollow structural microspheres were fabricated through an environmental friendly hydrothermal carbon templating approach with subsequently annealing process in air, where carbon spheres plays as template to create void space, and that promote metal source loading into colloidal carbon sphere. The resultant hollow $MgFe_2O_4$ sphere possess excellent textural properties of a large void space size (50-80nm) and tailored shell thickness(25-35nm). The spinel $MgFe_2O_4$ hollow structural microspheres used as an anode material for rechargeable lithium-ion battery possesses a high initial discharge specific capacity of 616.3 mAh g^{-1} at a stable current density of 500 mAh g^{-1} and the capacity retention of 559.9 mAh g^{-1} by 18 cycles. The excellent electrochemical performances of the spinel $MgFe_2O_4$ hollow structural microspheres may be associated with the special porous hollow structures, which deliver an easy Li^+ diffusion pathway and facilitate charge transfer and alleviate the volume variation and diminishes polarization in cycling.

Keywords: Hollow microspheres; Magnesium ferrite; Photocatalytic material; Hydrothermal

1. INTRODUCTION

The ever-increasing energy demand are primary driving forces for the exploitation of environmental friendly renewable energy storage materials. Among different energy store apparatus, lithium-ion batteries (LIBs) have displayed superior electrochemical performances in terms of high battery voltage, long recycle life, low self-discharge, no memory effects, high energy ratio power and energy densities, and environmental friendliness[1]. The currently commercialized graphite anode has some interesting performance, for example lower working voltages *versus* Li, long recycle life, and lower cost. However, its main disadvantage is its low theoretical specific capacity of 372 mAh g^{-1}, which has restricted the further development of LIBs[2]. In order to attain the high power and high

energy density demand of LIBs, electrode materials with large specific capacities, battery voltages, and Li diffusion coefficients are required.

Spinel ferrites $MgFe_2O_4$, a soft magnetic n-type semiconductor material with normal spinel-type cubic structure[3], has been examined as potential anode for LIBs. Recently, Sivakumar fabricated nanostructured $MgFe_2O_4$ via sintering the mixture of α-Fe_2O_3 and MgO, and surveied its behavior as an anode material for LIBs, the specific capacity rapidly decreased through 10 cycles is 300 mA g^{-1}, which can not meet the actual application requirements[4]. The fast capacity fading and low rate performance, which caused by the large volume expansion during Li^+ insertion/extraction, agglomeration, and intrinstic low electrical conductivity, hamper its applications. Recently, intensive efforts have dedicated to solve these problems. Gong synthesized carbon-coated $MgFe_2O_4$ nanoparticles and exhibited a high specific capacity of 466 mA h g^{-1} at a great current density of 1600 mA g^{-1} and a higher rate capability than the regular $MgFe_2O_4$ nanoparticles[5]. Then, Pan prepared $MgFe_2O_4$ by sol-gel method and after 50 cycles the capacity was 291 mAh g^{-1} at 450 mA g^{-1} current density[6]. The poor rate and cycling stability leaves huge challenging for excellent anode materials.

Construction of inorganic hollow microspheres materials have attracted growing interest over the years because of their controllable shape, uniform size, high specific surface area, low density, and shells permeability properties[7-10], which endows them with widespread potential application in LIBs[11-13]. Recently, zero, one, two and three-dimensional $MgFe_2O_4$ nanostructure materials with different morphologies, such as nanoparticles[17], nanofibers[14], and microspheres[15] have been developed by combustion[18], ball milling[14], sol-gel[17], electrospinning[19], and hydrothermal[20] methods. However, previous work has rarely addressed the magnesium ferrite hollow structured microspheres, therefore, searching an easy method for the preparation of hollow morphology magnesium ferrite nanostructure is urgently needed.

In the present work, we report a facile and green solvothermal carbon templating approach for the fabrication of hollow $MgFe_2O_4$ microspheres with high surface area. The spinel $MgFe_2O_4$ hollow structural microspheres used as an anode material for LIBs possesses a high initial discharge specific capacity of 616.3 mAh g^{-1} at a stable current density of 500 mAh g^{-1} and the capacity retention of 559.9 mAh g^{-1} by 18 cycles. The hollow microspheres offer adequate void space developed during thermal annealing treatment, conducive for electrolyte penetration and accelerate electron transfer and tolerate the volume change upon prolonged charge/discharge cycling. And the possible preparation mechanism of the hollow microspheres was also illustrated meanwhile.

2. EXPERIMENTAL SECTION

2.1. Materials

Glucose and $Mg(Ac)_2.4H_2O$, $Fe(NO_3)_3$, and NH_4Ac of analytical purity were obtained from Aladdin Chemical Corporation. Ethylene glycol (EG) of analytical purity was purchased from Beijing Chemical Corporation.

2.2. Synthesis

Synthesis of hollow $MgFe_2O_4$ microspheres: the prepared carbon spheres with a uniform morphology size at 300 nm were synthesized via hydrothermal method and played as templates. In a typical synthesis for the $MgFe_2O_4$ hollow spheres, 0.8 g NH_4Ac, 1.62 g $Fe(NO_3)_3$, and 0.214 g $Mg(Ac)_2.4H_2O$ were added to 60.0 ml EG to form a suspension with vigorous stirring. Then, 0.2 g prepared nanocarbon spheres were added into the aqueous solution with the helping of ultrasonication for 30 min. Subsequently, the mixed black suspended solution was placed in a 100 ml teflon-sealed stainless autoclave and maintained in oven at 180 ℃ for 12 h. After a natural cooling to room temperature, the precursor was obtained via centrifugation and washed three times with the aid of absolute ethanol and deionized water, subsequently dried in oven at 80 ℃ for 6 h. Furthermore, a calcination process at 500 ℃for 2 h was carried out and the templates of carbon spheres were decomposed, resulting in the hollow $MgFe_2O_4$ microspheres.

2.3. Characterization

The crystal structure of the sample was examined by a Japan D/max-rB X-ray diffractometer with Cu-Ka radiation (λ=1.5418 Å). The thermogravimetric analysis (TGA) plot of C-$MgFe_2O_4$ precursor absorbed composites was performed using a China ZCT-2000 apparatus with a temperature rate of 10 ℃/min under air atmosphere. The morphologies of the samples were observed with a JSM-6700F scanning electron microscope and JEM-2010 transmission electron microscope, respectively. The chemical states of the hollow $MgFe_2O_4$ microspheres were obtained by a Thermo ESCALAB 250 X-ray photoelectron spectrometer. Fourier-transform infrared (FTIR) spectra were examined in the range 4000-450 cm^{-1}on a Nicolet Nexus-670 FT-IR spectrometer. In addition, the magnetization measurements were analyzed by a TMVSM 1230-HHHS vibrating sample magnetometer with a maximum applied field of 15 kOe.

2.4. Electrochemical measurements

The working electrodes were formed by mixing the slurry of active material(75wt%), conductivity agent (acetylene black, Super-P-Li)(15wt%), and polymer binder (polyvinylidene difluoride, PVDF, Aldrich)(10wt%) and disolving in N-methylpyrrolidone (NMP). Lithium foil was served as both the counter electrode and the reference electrode. The electrolyte solution was prepared by mixing 1 M $LiPF_6$ in a mixture of ethylene carbonate (EC) and diethyl carbonate (DEC) (1:1 by volume). The cell assembly was completed in an Arfilled glove box full of argon with water contents and oxygen concentrations less than 1 ppm. Galvanostatic charge-discharge of the cells was conducted through a LAND-CT2001A battery test system between a voltage window of 0.01 and 3.0 V at various current rates.

3. RESULTS AND DISCUSSION

Figure 1a. show the XRD data of the hollow $MgFe_2O_4$ spheres. All the diffraction peaks are in accordance with the spinel cubic $MgFe_2O_4$ phase (JCPDS card no. 73-1960).

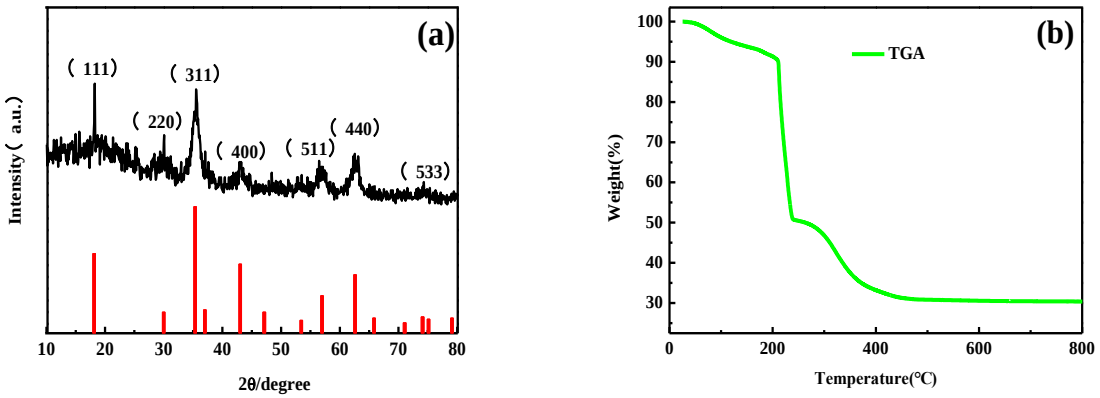

Figure 1. (a) the typical XRD pattern of the as-prepared $MgFe_2O_4$ composites, (b) the TGA curve of the precursor.

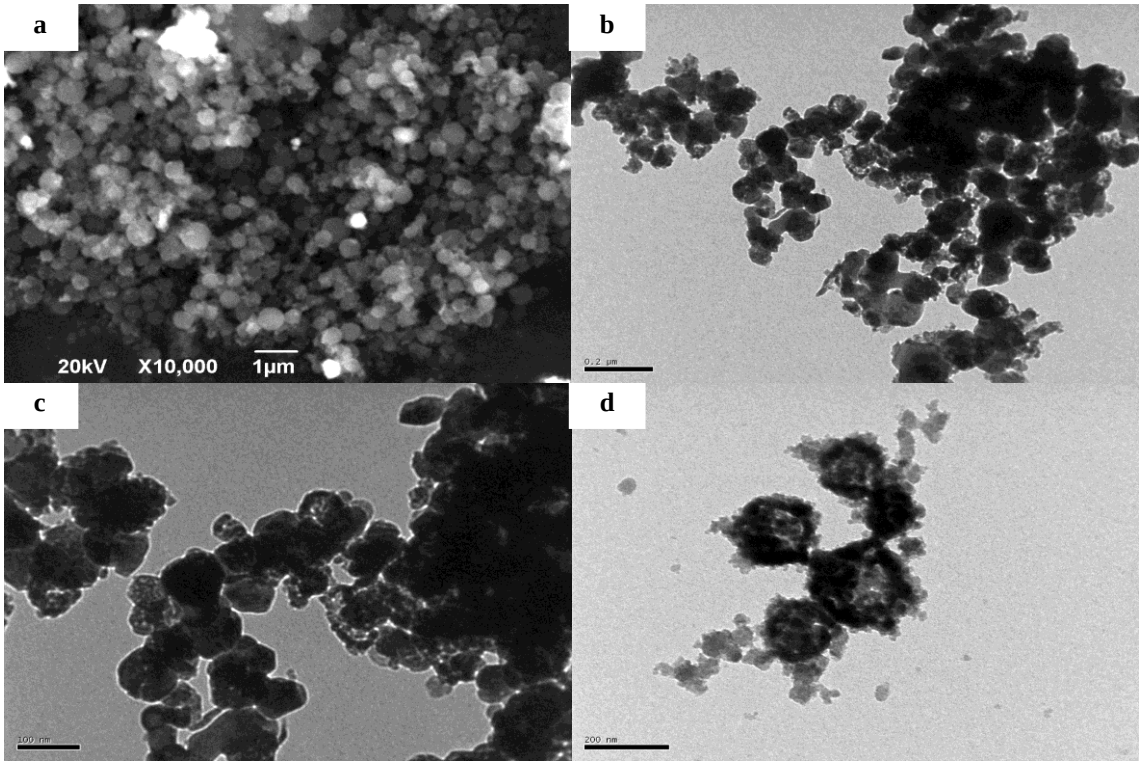

Figure 2. (a) SEM image of absorbed C-$MgFe_2O_4$ precursor, (b) TEM image of (a); (c) low- and (d) high magnification TEM images of the resultant hollow $MgFe_2O_4$ spheres.

All diffraction peaks can be indexed to the typical spinel structured $MgFe_2O_4$, the characteristic peaks in the $MgFe_2O_4$ pattern at 18.3°, 30.1°, 35.5°, 43.2°, 57.0°,62.6° and 74.1° are corresponding to (111), (220), (311), (400), (511), (440) and (533) reflections, respectively. No additional peaks of

impurity phase have been detected in the spectra, demonstrating the fabrication of a purely spinel cubic $MgFe_2O_4$ crystalline. The strong and narrow diffraction patterns revealed the well crystallized sample. Figure 1b. shows the TGA of C-$MgFe_2O_4$ precursor absorbed composites.

The image shows two steps of weight loss : the first minor loss step from 30 up to around 200 °C was due to the loss of adsorbed water molecules and trapped water molecules[6]; then a drastic mass loss in the range 200-455 °C, this weight lose is related to the metal absorbed composites converted into metal oxides and the hollow structure final fabricated with the carbon templates removed[16]. After 450 °C, any weight losses are not found, indicating that the templates have been burnt out. So the calcination temperature of absorbed C-$MgFe_2O_4$ precursor was set at 500 ℃ to make sure the carbon templates completely removed and the hollow $MgFe_2O_4$ spheres formed.

The spherical shape morphology of absorbed C-$MgFe_2O_4$ precursor, which were confirmed from the SEM and TEM technique, are shown in Figure 2a. and b. Figure 2a. presents the SEM image of absorbed C-$MgFe_2O_4$ precursor consists of well-dispersed, uniform and solid spherical structure which implies that the shape and the size of absorbed C-$MgFe_2O_4$ precursor is determined by the morphology of the carbon spheres templates[16]. From the typical SEM image, it is observed that the diameter of the absorbed C-$MgFe_2O_4$ precursor spheres are about 200 nm. Figure 2b. shows the TEM images of the absorbed C-$MgFe_2O_4$ precursor, form which the well-distributed spherical microstructure is also inferred. It is well identical with SEM result. The spheres displayed in both Figure 2a. and b. possess sleek surface, confirming the metal source ions and nucleates completely adsorpted into mesopores carbon spheres in the above possible synthesis mechanism of the hollow microspheres in Figure 5. The low- and high magnification TEM image of the resultant $MgFe_2O_4$ hollow spheres are shown in Figure 2c. and d. Figure 2c. presents the low-magnification TEM image of the resultant $MgFe_2O_4$ hollow spheres consists of well-dispersed, uniform and solid spherical structure which implies that the appearance and the size of final production is determined by the morphology of the carbon spheres templates. The obvious contrast of the dark edge and the pale center reveal the hollow nature of the resultant $MgFe_2O_4$ hollow spheres. Figure 2d. presents the high magnification TEM image of the resultant $MgFe_2O_4$ hollow spheres consists of an shell that was consist of plenty of small nanoparticles and an innercavity. The diameter of the typical hollow $MgFe_2O_4$ spheres is approximately 100 nm, which is smaller than that of absorbed C-$MgFe_2O_4$ precursor. The contraction may be caused by the carbon templates removal of absorbed C-$MgFe_2O_4$ precursor during calcination resulting the dense of the precursor to form the final hollow structure.

To verify the elemental composition and chemical state, $MgFe_2O_4$ microspheres were investigated by X-ray photoelectron spectroscopy (XPS). The survey spectrum Figure 3a. confirms the presence of Mg,Fe, O and C and no other elements in the composition. From Figure 3b. the Mg 1s spectra is observed at 1303.2 eV, which indicates the oxidation state of Mg^{2+}. Figure 3c. spectrum exhibits the binding energies at 725.6 and 710.6 eV for Fe $2p_{1/2}$ and Fe $2p_{3/2}$, which are due to the existance of Fe^{3+}. And the peak at 718.9eV is the shake-up satellite structure[18]. Figure 3d. the energy difference at 529.2 eV is correspond to the O 1s region, and the asymmetrical summit can be deconvoluted into two distinct peaks with binding energies of 528.5 and 530.7 eV, which are ascribed to the surface oxygen vacancies (O^{2-}) and OH group or H_2O absorbed onto the $MgFe_2O_4$ microspheres surface[19], respecively. Due to the specimen has been dried up before the test, the reason for the nice

adsorption performance of the hollow $MgFe_2O_4$ microspheres may be related to its numerous mesopores on the shell of the hollow microspheres, which can promote the transportation of Li^+ and relieve the large volume expansion in Li^+ insertion/extraction process[20-22]. The exsitance of C 1s peak located in 284.6 eV is used as reference to calibrate the acquired spectra. The XPS results are consistent with the XRD analysis and confirms the formation of crystalline $MgFe_2O_4$ hollow microspheres.

The chemical bonds of $MgFe_2O_4$ were investigated by the FTIR spectrum (Fig. 4a). The absorption bands at 560 and 437 cm^{-1} corresponded to the stretching vibrations at the tetrahedral and octahedral sites, respectively, which suggests the intrinsic metal-oxygen stretching frequencies[23]. The band at 1627 cm^{-1} are due to the surface absorbed moisture. The peaks around 3440 cm^{-1} are ascribed to the hydroxyl. The peaks at 2368 cm^{-1} are in accordance with CO_2 adsorbed from the atmosphere[24]. The bands at 1452 cm^{-1} may be assigned to the C-H vibration , which was corresponded to the residual EG traces[25].

The magnetic hysteresis curve for the present hollow magnesium ferrites is shown in Fig. 4b. The saturation magnetization value was 19.2 emu/g, which ensured the magnetic materials can be collected and recycled from solution by applied external magnetic field[26, 27].

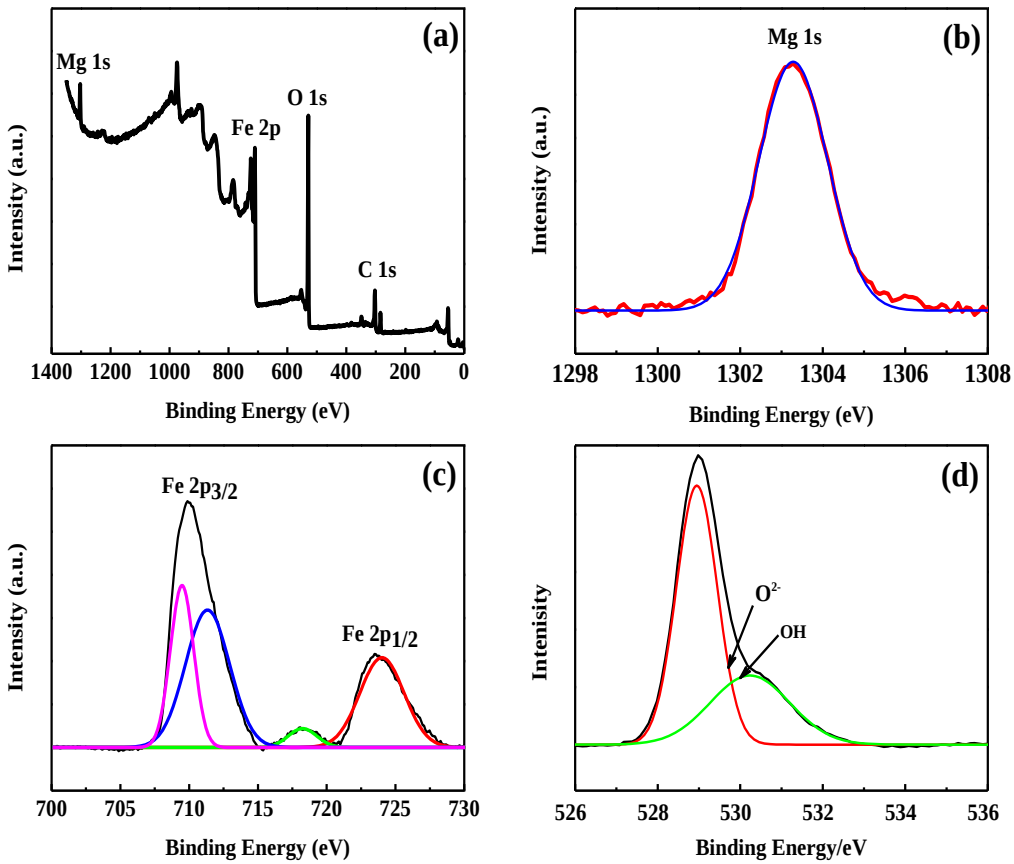

Figure 3. XPS spectra of (a) survey of the sample, (b) Mg 1s, (c) Fe 2p, (d) O 1s for the hollow $MgFe_2O_4$ microspheres

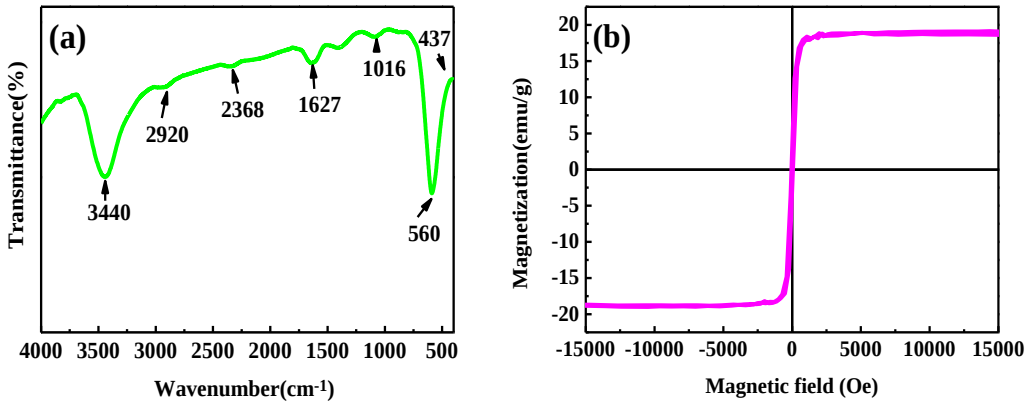

Figure 4. FTIR spectra (a) and magnetization curve (b) of the hollow $MgFe_2O_4$ microspheres

The schematic route of hollow $MgFe_2O_4$ microspheres is depicted in Fig. 5. The formation process of hollow $MgFe_2O_4$ microspheres: (i) making the metal source ions and nucleates completely adsorpted into mesopores carbon spheres with the assistance of -OH and -COOH functional groups on its surface and the porous structure[17]; (ii) during annealing process in air, templates removed and the compact oxide shell formed and finally the hollow structure prepared.

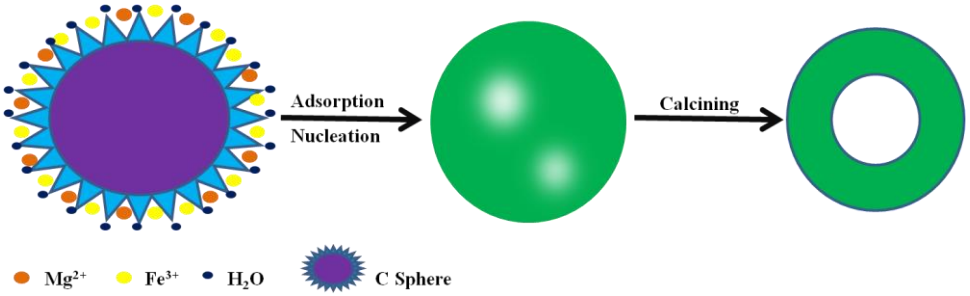

Figure 5. Schematic illustrations of the formation process of $MgFe_2O_4$ hollow microspheres

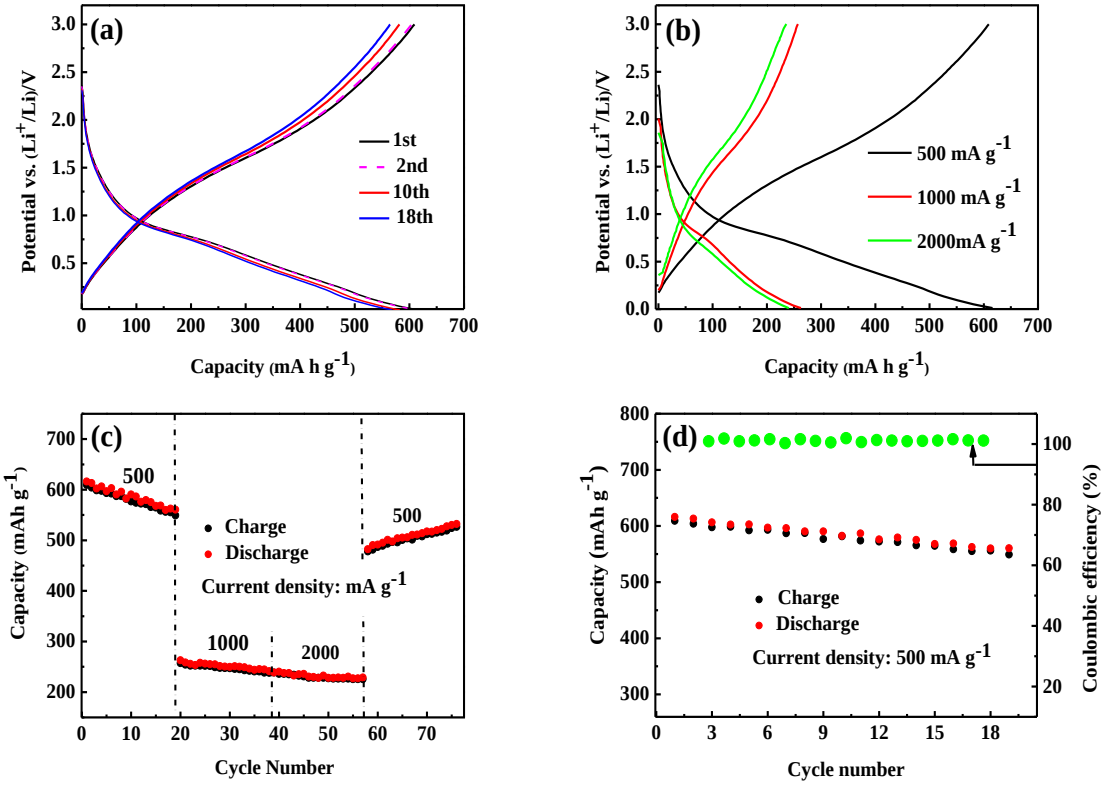

Figure 6. Electrochemical performance of the hollow $MgFe_2O_4$ microspheres: (a) discharge and charge profiles for the 1st, 2nd, 10th, 18th, cycles at 500mA $g^{-1}$of, (b) discharge and charge curves under different current densities, (c) rate capacity at current densities of 500, 1000, 2000 mA g^{-1} current density, (d) discharge/charge capacity and coulombic efficiency vs. cycle number at a 500 mA g^{-1} current density.

Table 1. Comparision of the cycling performance of different $MgFe_2O_4$ micro/nanostructures.

Material	Reversible capacity (mAh g^{-1})	Cycles	Ref
$MgFe_2O_4$ nanoparticles	291 (450 mA g^{-1})	50	[6]
$MgFe_2O_4$/reduced grapheme oxide composites	197.6 (500 mA g^{-1})	5	[28]
Nanostructured $MgFe_2O_4$	300	10	[4]
The hollow $MgFe_2O_4$ microspheres	559.9 (500 mA g^{-1})	18	This work

The electrochemical performance of the hollow $MgFe_2O_4$ microspheres as the anode material for LIB was investigated by galvanostatic discharge/charge tests. Figure 6a. indicates the results of the typical galvanostatic charge-discharge profiles of the product at a current density of 500 mA g^{-1} over the potential scope of 3.0-0.01 V during the 1st, 2nd, 10th and 18th cycles. During the first discharge process, the electrode displayed a obvious potential plateau at about 0.75 V. The discharge capacities

were 616.3, 613.0, 582.6 and 559.9 mAh g^{-1} for the 1st, 2nd, 10th and 18th cycles, respectively. The corresponding charge capacities were 609.3, 604.0, 581.7 and 556.2 mAh g^{-1}. It can be noticed that the discharge and charge curves have analogous shapes. A good overlap is found between the 1st, 2nd, 10th and 18th cycles, which strongly suggests a possibility of the good reversibility of the hollow $MgFe_2O_4$ microspheres electrode. Figrue 6b. displays the results of the discharge/charge curves of the hollow $MgFe_2O_4$ microspheres with various current densities. It is easy to find that the tendencies of the curve at different current densities are almost unchanged, except for the shorter potential platform with smaller specific capacities. Figure 6c. shows the rate performance of the hollow $MgFe_2O_4$ microspheres at 500, 1000 and 2000 mA g^{-1} current densities. It can be noticed that the hollow $MgFe_2O_4$ microspheres delivers the reversible capacities of 560.4, 241.2 and 227.1 mAh g^{-1} at the current densities of 500, 1000 and 2000 mA g^{-1}, respectively. The capacity revives to about 482.3 mAh g^{-1} when the current density regains back to 500 mA g^{-1}. The result exposes that the hollow $MgFe_2O_4$ microspheres possesses a great rate capability and structure stability even at very higher current densities. Figure 6d. exhibits the cycling performance and columbic efficiency of the hollow $MgFe_2O_4$ microspheres anodes at a current density of 500 mA g^{-1}. After 18 cycles, the specific capacity stabilizes at around 559.9 mAh $g^{-1}$with a columbic efficiency of nearly 97% under the following cycling process, demonstrating the great capacity retention. It is obvious that the hollow $MgFe_2O_4$ microspheres displayed upgraded cycling performance and promoted specific capacity. Recently, Pan[6], prepared $MgFe_2O_4$ by sol-gel method which displayed a capacity of 590 mAh $g^{-1}$and after 50 cycles the capacity has further decay to 291 mAh g^{-1} at 450 mA g^{-1} current density, however, the hollow $MgFe_2O_4$ microspheres shows a stable capacity of 559.9 mAh g^{-1} even after 18 cycles. To illustrate the excellent cycling performance of the hollow $MgFe_2O_4$ microspheres, a detailed comparison on the hollow $MgFe_2O_4$ microspheres with previous reported various $MgFe_2O_4$ micr/nanostructures was summarized in Table 1. Obviously, the hollow $MgFe_2O_4$ microspheres shows excellent structure stability and significant improvement reversible capacity in cycling performance.

4. CONCLUSIONS

In summary, spinel MgFe2O4 hollow structural microspheres were fabricated through an environmental friendly hydrothermal carborn templating approach with subsequently annealing process in air, where carbon spheres plays as template to create void space, and that promote metal source loading into colloidal carbon sphere. The resultant hollow $MgFe_2O_4$ sphere possess excellent textural properties of a large void space size (50-80nm) and tailored shell thickness(25-35nm). The spinel $MgFe_2O_4$ hollow structural microspheres used as an anode material for rechargeable lithium-ion battery possesses a high initial discharge specific capacity of 616.3 mAh g^{-1} at a current density of 500 mAh g^{-1} and the capacity retention of 559.9 mAh g^{-1} by 18 cycles. The excellent electrochemical performances of the spinel $MgFe_2O_4$ hollow structural microspheres may be associated with the unique porous hollow structures, which deliver an easy Li^+ diffusion pathway and facilitate electron transfer and alleviate the volume variation and diminishes polarization in cycling. The hollow microspheres offer adequate void space developed during thermal annealing treatment, conducive for electrolyte

penetration and accelerate electron transfer and tolerate the volume change upon prolonged charge/discharge cycling. And the present method can also be greatly applied to fabricate other metal oxides with well-defined hollow structures and improved performances.

ACKNOWLEDGMENTS
The authors acknowledge the financial support from the National Natural Science Foundation of China (Grant No. 11602233).

NOTES
The authors declare no competing financial interest.

References

1. S. Yuvaraj, R.K. Selvan and S.L. Yun, *Rsc Advances.,* 6 (2016) 21448.
2. G. Sandi, *International Symposium on New Materials for Electrochemical Systems.,* 4 (2001) 259.
3. V. Šepelák, A. Feldhoff, P. Heitjans, F. Krumeich, D. Menzel, F.J. Litterst, I. Bergmann and K.D. Becker, *Chemistry of Materials.,* 18 (2006) 3057.
4. N. Sivakumar, S.R.P. Gnanakan, K. Karthikeyan, S. Amaresh, W.S. Yoon, G.J. Park and Y.S. Lee, *Journal of Alloys & Compounds.,* 509 (2011) 7038.
5. C. Gong, Y.J. Bai, Y.X. Qi, N. Lun and J. Feng, *Electrochimica Acta.,* 90 (2013) 119.
6. Y. Pan, Y. Zhang, X. Wei, C. Yuan, J. Yin, D. Cao and G. Wang, *Electrochimica Acta.,* 109 (2013) 89.
7. K. Zhang, Y. Lin, C. Wang, B. Yang, S. Chen, S. Yang, W. Xu, H. Chen, W. Gan and Q. Fang, *The Journal of Physical Chemistry C.,* 120 (2016) 13120.
8. Y. Zhao and L. Jiang, *Advanced Materials.,* 21 (2009) 3621.
9. Y.w. Jun, J.s. Choi and J. Cheon, *Angewandte Chemie International Edition.,* 45 (2006) 3414.
10. Q. Xie, F. Li, H. Guo, L. Wang, Y. Chen, G. Yue and D.-L. Peng, *ACS applied materials & interfaces.,* 5 (2013) 5508.
11. Q. Wang, L. Jiao, Y. Han, H. Du, W. Peng, Q. Huan, D. Song, Y. Si, Y. Wang and H. Yuan, *The Journal of Physical Chemistry C.,* 115 (2011) 8300.
12. X. Wang, X.L. Wu, Y.G. Guo, Y. Zhong, X. Cao, Y. Ma and J. Yao, *Advanced Functional Materials.,* 20 (2010) 1680.
13. G. Zhangand X.W. Lou, *Angewandte Chemie International Edition.,* 53 (2014) 9041.
14. S. Maensiri, M. Sangmanee and A. Wiengmoon, *Nanoscale research letters NRL.,* (2009).
15. D. Kang, X. Yu, M. Ge and W. Song, *Microporous and Mesoporous Materials.,* 207 (2015) 170.
16. X. Jiang, L. Yu, C. Yao, F. Zhang, J. Zhang and C. Li, *Materials.,* 9 (2016) 323.
17. X. Sun and Y. Li, *Angewandte Chemie International Edition.,* 43 (2004) 597.
18. J. Lu, X. Wei, Y. Chang, S. Tian and Y. Xiong, *Journal of Chemical Technology & Biotechnology.,* 91 (2016) 985.
19. Z. Zheng, J. Teo, X. Chen, H. Liu, Y. Yuan, E.R. Waclawik, Z. Zhong and H. Zhu, *Chemistry - A European Journal.,* 16 (2010) 1202.
20. M. Wang, H. Yang, X. Zhou, W. Shi, Z. Zhou and P. Cheng, *Chemical Communications.,* 52 (2015) 717.
21. S. Hao, B. Zhang, S. Ball, B. Hu, J. Wu and Y. Huang, *Materials & Design.,* 92 (2016) 160.
22. R. Jin, G. Liu, C. Liu and L. Sun, *Materials Research Bulletin.,* 80 (2016) 309.
23. Y. Shen, Y. Wu, X. Li, Q. Zhao and Y. Hou, *Materials Letters.,* 96 (2013) 85.
24. X. Ma, H. Sun, H. Hong and M. Zheng, *Catalysis Letters.,* 119 (2007) 142.
25. X. Wang, X.L. Wu, Y.G. Guo, Y. Zhong, X. Cao, Y. Ma and J. Yao, *Advanced Functional Materials.,* 20 (2010) 1680.

26. D. Chen, Y. Zhang and C. Tu, *Materials Letters.,* 82 (2012) 10.
27. N.R. Su, P. Lv, M. Li, X. Zhang, M. Li and J. Niu, *Materials Letters.,* 122 (2014) 201.
28. X. Zhang, T. Chen, D. Yan, W. Qin, B. Hu, Z. Sun and L. Pan, *Electrochimica Acta.,* 180 (2015) 616.